This is the accepted manuscript made available via CHORUS. The article has been published as:

Output polarization characteristics of a GaN microcavity diode polariton laser

Aniruddha Bhattacharya, Md Zunaid Baten, Ivan Iorsh, Thomas Frost, Alexey Kavokin, and Pallab Bhattacharya

Phys. Rev. B **94**, 035203 — Published 25 July 2016
DOI: 10.1103/PhysRevB.94.035203

Output Polarization Characteristics of a GaN Microcavity Diode Polariton Laser

Aniruddha Bhattacharya[1], Md Zunaid Baten[1], Ivan Iorsh[2,3], Thomas Frost[1],
Alexey Kavokin[4,5,6], and Pallab Bhattacharya[1*]

[1]*Center for Photonics and Multiscale Nanomaterials,*
Department of Electrical Engineering and Computer Science, University of Michigan,
1301 Beal Avenue, Ann Arbor, MI 48109, USA
[2]*National Research University for Information Technology, Mechanics and Optics (ITMO), St. Petersburg 197101, Russia*
[3]*Division of Physics and Applied Physics, Nanyang Technological University 637371, Singapore*
[4]*CNR-SPIN, Viale del Politecnico 1, I-00133, Rome, Italy*
[5]*School of Physics and Astronomy, University of Southampton, SO17 1BJ Southampton, United Kingdom*
[6]*Spin Optics Laboratory, State University of Saint-Petersburg, 1, Ulianovskaya, 198504, St-Petersburg, Russia*
[*]Email: pkb@umich.edu

We report the steady state output polarization characteristics of GaN-based microcavity polariton lasers operated with electrical injection at room temperature. The output is unpolarized below the non-linear threshold injection current and is linearly polarized above it with a maximum degree of polarization of ~ 22 %. The results have been analyzed theoretically and the calculated results are in agreement with the measured data. We have also measured the polarization resolved output light-current characteristics, wherein a distinct lowering of the non-linear threshold is observed in one device. This is interpreted in terms of spatially inhomogeneous lifting of degeneracy and polarization splitting in the microcavity.

A stable linearly polarized coherent ultraviolet (UV) or deep UV light source is required for biochemical analysis, photo-alignment of nematic liquid crystals, eye surgery, and other industrial applications [1]. A single source or an array, to get higher powers, would be adequate for such applications. Current planar GaN-based UV lasers have threshold currents ~ 10 kA/cm^2 or higher. A polariton laser is an inversionless coherent light source [2-3] operating in the strong coupling regime of light-matter interaction [4-6]. Exciton-polariton lasers have been realized with suitable semiconductor microcavities with both optical and electrical pumping [7-24]. Coherent emission is produced by spontaneous radiative recombination from a macroscopic, coherent and degenerate exciton-polariton condensate, often termed a Bose-Einstein condensate or BEC [11, 12, 25, 26]. In the case of polariton lasers, the system is in a metastable condensed state in which the polaritons are only in equilibrium among themselves and not with the semiconductor lattice. Thus, although the redistribution of polaritons in momentum space above the condensation threshold does not conform to equilibrium Bose-Einstein statistics, nevertheless the bimodal distribution of polaritons which develops above threshold have many of the properties of BECs. The non-linear threshold of a polariton laser is lower than that of a conventional photon laser because the former does not require the inversion of electronic population and quantum degeneracy may be reached at very low polariton densities. The bosonic behavior of the degenerate state, or polariton ground state, has been verified by several elegant experiments [3, 7-26]. An important characteristic of the output of a polariton laser is its polarization [11-12, 25, 27-35]. Below the non-linear threshold, the optical output is essentially unpolarized [11-12, 14, 21, 25, 32, 34-35]. As the non-linear threshold is reached, there is spontaneous build-up of linear polarization in the emission spectra, which is a consequence of spontaneous symmetry breaking in the degenerate condensate [25, 28-30, 33-34]. The linear polarization results from a breaking of the ground state degeneracy into two closely spaced states. Above threshold the condensate occupies the lower of these two states and the linear polarization of the emission corresponds to this state.

In all the reported experiments [3, 11-12, 14, 25, 31, 34-35], except one with a GaAs-based microcavity at 30 K [21], the device has been excited with linearly or circularly polarized light. We report here the first experimental study of the output polarization characteristics of a GaN-based electrically pumped microcavity polariton laser. We have studied electrically pumped bulk GaN microcavity polariton lasers operated at room temperature [24, 36-37]. The devices are characterized by a threshold current density in the range of J_{th}=125 A/cm^2 to 375 A/cm^2 , a detuning ranging from -4 meV to -13 meV and a strong coupling in the microcavity characterized by a Rabi splitting of 33.9 to 35.5 meV. The formation of a degenerate condensate is observed in the angular resolved electroluminescence data. In particular, we have investigated the steady state linear polarization build up, caused by polarization pinning, in the output of multiple devices. It is observed that the emission is unpolarized below the non-linear threshold and is linearly polarized above it with a maximum polarization of ~ 22 %. For higher injection currents, the degree of polarization decreases. It is also observed that in one device the non-linear threshold for the linear polarization resolved output is significantly lower than that for the unresolved output, a hitherto unobserved phenomenon, which possibly indicates that the microcavity may be spatially inhomogeneous and the polarization splitting is different in different domains [38, 39].

In the present study, we have characterized several identical electrically pumped bulk GaN-based microcavity polariton lasers fabricated from a single epitaxially grown heterostructure sample shown in Fig. 1(a). Device fabrication is described in the Supplemental

Material [40] and the device is shown schematically in Fig. 1(b). Since the device cross-section is fairly small, any difference in the measured characteristics between the devices is expected to arise from the number of defects in the active region. The defect density in the active region is 6.1 x 10^8 cm^{-2} [37]. All measurements reported here have been done at room temperature. The microcavity quality factor, Q, and the corresponding cavity mode lifetime, τ_c, are determined to be ~ 1700 and ~ 0.3 ps, respectively, from room temperature microphotoluminescence measurements (see Supplemental Material [40]). The microphotoluminescence data is shown in Fig. 1(c). Angle-resolved electroluminescence measurements were made to ascertain the strong coupling regime of operation of the devices and to determine the polariton dispersion characteristics and are described in the Supplemental Material [40]. The measurements were carried out at a low value of continuous wave (CW) current injection (later confirmed to be 0.95 J_{th}, where J_{th} is the non-linear threshold to be described later). From the analysis of the measured sub-threshold lower polariton (LP) dispersion characteristics, in the framework of the 2x2 coupled harmonic oscillator model, the cavity-to-exciton detuning δ and vacuum-field Rabi splitting Ω of two devices are found to be in the ranges of -4 meV to -13 meV and 33.9 meV to 35.5 meV, respectively. The dispersion curves are calculated assuming the exciton linewidth of 6 meV. In the following, the polariton lasing features are described in more detail.

The output light-current (L-I) characteristics of the devices were determined by recording the electroluminescence in the direction normal ($k_{||}$~0) to the Bragg mirrors (zero angle), as a function of continuous wave injection current. The LP emission intensities were recorded by a photomultiplier tube after spectrally filtering the output luminescence through an imaging monochromator. The output power was also directly measured with an optical power meter at sufficiently high injections above threshold. Both techniques yielded identical trends. As shown in Fig. 2(a), a non-linear threshold signaling the onset of stimulated scattering is observed at a current density of J_{th}=262.5 A/cm^2 which is close to the value reported previously in similar devices [24, 36-37]. The corresponding LP density at threshold is 3.88 x 10^{16} cm^{-3}, calculated with an excitonic radiative recombination lifetime of 0.71 ns. The non-linear region of the electroluminescence is characterized by a slope of ~13.7 and the enhancement of the output coherent luminescence over the active lasing regime is ~ 3.5 orders of magnitude. Both values are comparable to the corresponding characteristics of the best optically pumped CdTe-based, GaAs-based and GaN-based polariton lasers reported in the literature [3, 7-9, 11-15, 20] and are significantly better than those reported for electrically pumped devices [21, 22, 24, 36-37]. The onset of non-linearity and threshold are accompanied by an abrupt reduction of the LP emission linewidth and a blue-shift of the LP electroluminescence peak energy (~ 8 meV) shown in Figs. 2(b) and (c), respectively. The minimum measured emission linewidth is ~ 870 μeV, which corresponds to a LP coherence time of ~ 4.8 ps. The spontaneous radiative recombination lifetime of the lower polaritons in the condensate is estimated as $\tau_{LP} = \tau_C / |C(k_{||} = 0)|^2 = 0.6$ ps. With further increase of the injection current, the transition from strong coupling to weak coupling takes place and at J = 36.8 kA/cm^2 conventional photon lasing due to population inversion is observed. The two-threshold lasing behavior is shown in Fig. 2(d). The polariton occupation in momentum space at different injection levels was also measured by angle-resolved electroluminescence in several devices. The occupation is calculated from the output power measured with an optical power meter after spectrally filtering the part of the electroluminescence spectrum centered on the lower polariton resonances. The polariton occupation number per $k_{||}$ state is calculated using the relation, $I_{LP} = \frac{\eta n_{LP}^{\infty}(k_{||}) |C(k_{||})|^2 Mhc}{\tau_C \lambda}$ [21], where η is the collection efficiency, $\tau_C / |C(k_{\|})|^2$ is the spontaneous radiative recombination lifetime of the lower polaritons, M is the number of transverse states included in the detection cone, and $|C(k_{\|})|^2$ is the photon fraction at a wave vector $k_{\|}$. The number of states within the detection cone is given by $M = D^2 / 16 (k_o \Delta\theta)^2$, where D is the diameter of the emission spot, $k_o = 2\pi / \lambda$ (the free-space wave number) and $\Delta\theta$ is the detection half angle. The polariton condensate occupation numbers are very similar in all the devices. Representative data are shown in Fig. 2(e). A random and non-thermal LP occupation below threshold transforms to a peaked occupancy at $k_{\|}$~0 above threshold, signaling the formation of a coherent bosonic condensate. There is no evidence of a relaxation bottleneck at any injection [24, 36-37].

We measured the degree of linear polarization of the polariton emission in the normal direction ($k_{\|}$ ~ 0) (see Supplemental Material [40]) as a function of injection current in multiple devices. Figure 3(a) is a plot of the electroluminescence intensity as a function of the angle of the linear analyzer. Below the non-linear threshold, the emission is depolarized. Above threshold, a maximum linear polarization of ~ 22 % is recorded for an injection level of 275 A/cm$^{2.}$ The linear polarization is found to be preferentially oriented along the $[1\bar{1}00]$ crystallographic axis in all the devices. Figures 3(b) and (c) depict the measured steady state linear polarization of the output LP electroluminescence as a function of the injection current for two devices. The output is essentially unpolarized below the threshold value, the degree of linear polarization being below the detection limit of the measurement system. At threshold, there is a sharp increase in linear polarization due to stimulated LP scattering from the unpolarized reservoir to the polarized seed condensate in the presence of a small linear polarization splitting [38]. This is followed by a peaking and a steady decrease at higher injection, which is the depinning effect also observed by Levrat *et al.* [34]. The depinning effect is a result of strong polariton-polariton repulsive interactions and self-induced Larmor precession of the Stokes vector of the condensate [33, 34]. The measured thresholds for linear polarization agree with the non-linear threshold in the light-current characteristics within the limits of experimental accuracy. Polarization-resolved light-current characteristics were also measured and are plotted alongside the polarization integrated characteristics for two devices in Figs. 3(d) and (e). The data of Device 2 in Fig. 3(e) indicate that the value of the threshold current density remains unchanged for the two cases within the experimental accuracy. In contrast, similar data for Device 1 shown in Fig. 3(d) indicate a reduction of the threshold current density of the polarization-resolved output by ~ 70 A/cm^2 compared to that of the polarization unresolved output as one can clearly see in the inset. This effect was only observed in one device, nonetheless during repeated measurements. It may be remembered that this device also exhibited the highest degree of non-linearity and strong coupling over a wide injection range. The lower threshold of a specific linear polarization resolved electroluminescence probably results from a spatially inhomogeneous polarization splitting in the GaN microcavity, similar to what has been observed before in a CdTe microcavity [38, 39]. Some parts of the sample may be characterized by a large splitting of the linearly polarized modes and a specific linear polarization build-up occurs with a lower threshold. In other domains the polarization splitting is negligibly small, resulting in emission which will be unpolarized in the steady state. The lowering of threshold observed here is less than the expected factor of 2 due to deviations in the microcavity characteristics from an ideal case. Nonetheless, this is the manifestation of inhomogeneity, probably arising from defects, in the linear polarization resolved electroluminescence of a polariton laser. Similar, albeit not identical, results have been observed in InGaAs microcavities, under non-resonant circularly polarized optical pulsed excitation, where the transition from the strong- to the weak-coupling regime takes place with increasing excitation at different powers for polaritons with opposite spin polarizations and is determined by the relative populations of the polaritons with opposite spin orientations [41,42].

We have analyzed the experimental results by modeling the kinetics of the system with the four coupled stochastic differential equations [33, 34].

$$\frac{d\psi_\sigma}{dt}=\frac{1}{2}\left[W(t)-\Gamma_c\right]\psi_\sigma+\frac{1}{2}(\gamma+i\Omega)\psi_{-\sigma}-\frac{i}{\hbar}\left[\alpha_1\left|\psi_\sigma\right|^2+\alpha_2\left|\psi_{-\sigma}\right|^2\right]\psi_\sigma+\theta_\sigma(t) \tag{1}$$

$$W(t)=a_{ph}N_r(t)+b_{pol}N_r^2(t) \tag{2}$$

$$\frac{dN_r}{dt}=-\Gamma_r N_r-W(t)\left[\left|\psi_-\right|^2+\left|\psi_+\right|^2+1\right]+W_e n_{e-h}(t) \tag{3}$$

$$\frac{dn_{e-h}}{dt}=\frac{J}{q}-\frac{n_{e-h}}{\tau_{e-h}}-W_e n_{e-h} \tag{4}$$

The order parameter $\psi_\pm$ describes the many body wavefunction of polariton condensates with +1 and -1 projections of spin to the structure axis, N_r is the exciton reservoir occupation, and $n_{e\text{-}h}$ is the occupation of the free carrier reservoir. $W(t)$ defines the rate of the polariton relaxation towards the ground state. We consider two relaxation mechanisms, namely the polariton-phonon scattering characterized by the scattering rate a_{ph} and polariton-polariton scattering with the rate b_{pol}. In all probability, the phonon scattering process (the first term on the right-hand side of equation (2)) does not involve a single scattering event but rather proceeds through a cascade of phonon emissions. Nevertheless, the phenomenon of final-state stimulation is present and for the rate of polariton-polariton scattering, it is proportional to square of the reservoir occupation as the rate of any two-body collision process. The first term in the right-hand side of equation (2) describes the phonon induced scattering of excitons and is linearly dependent on the exciton reservoir occupation. The two-body collision process is described by the second term in equation

(2) which is quadratic in the exciton reservoir occupation. Γ_c is inversely proportional to the polariton lifetime, which is mainly governed by the cavity quality factor. The constants Ω and γ correspond to the effective magnetic field leading to the energy splitting of the polarized condensate states and to the spin relaxation term, respectively. Constants α_1 and α_2 describe the interactions of polaritons with the same and opposite spin projections, respectively. Phenomenological constants Γ_r and W_e describe the decay rate of the excitons in the reservoir and the exciton formation rate, respectively.

The noise term $\theta(t)$ is defined by its correlators:

$$\left\langle \theta_\sigma(t)\theta_{\sigma'}(t') \right\rangle = 0 \tag{5}$$

$$\left\langle \theta_\sigma(t)\theta^*_{\sigma'}(t') \right\rangle = \frac{1}{2}W(t)\delta_{\sigma\sigma'}\delta(t-t') \tag{6}$$

The system of equations (1-4) is then numerically solved using the stochastic Runge-Kutta algorithm. For the numerical calculation we use the following parameters corresponding to conventional GaN -based laser diodes [43]: Γ_c= 1.3 ps^{-1}, γ= 0.0035 ps^{-1}, Ω = 0.03 ps^{-1}, α_1 =0.0001 ps^{-1}, α_2 = -0.1 α_1, a_{ph} = 10^{-11} ps^{-1}, b_{pol} = 10^{-12} ps^{-1}, Γ_r = 0.001 ps^{-1}, W_e = 0.01 ps^{-1}, τ_{e-h} = 2000 ps. The ground state occupation number is given by $n(t) = |\psi_+|^2 + |\psi_-|^2$ and the components of the condensate pseudospin linked to the output light polarization are:

$$S_x = \mathrm{Re}\left(\psi^*_+\psi_-\right) \tag{7}$$

$$S_y = \mathrm{Im}(\psi^*_+\psi_-) \tag{8}$$

$$S_z = \frac{1}{2}(|\psi_+|^2 - |\psi_-|^2) \tag{9}$$

Time and noise averaged signals have been recorded during the measurements. Namely the degree of linear polarization is given by $s_x = \left\langle \int dt S_x(t) / \int dt n(t) \right\rangle$, where brackets symbolize averaging over the noise. We next compare the results of the experiment and numerical simulations. Figure 2 (a) shows the calculated dependence of the condensate occupation number $n(t)$ on the injected current density alongside the measured data. Figure 3(b) shows the calculated dependence of the degree of linear polarization of the polariton laser emission on the pump current together with the measured data for Device 1. In order to obtain the theoretical values of the degree of linear polarization for Device 2, the following parameters have been varied with respect to the analysis for Device 1: the spin relaxation rate, γ , has been changed from 0.0035 ps^{-1} to 0.005 ps^{-1} , the polariton radiative rate Γ_c has been changed from 1.3 ps^{-1} to 1 ps^{-1} and the internal magnetic field Ω has been changed from 0.03 ps^{-1} to 0.05 ps^{-1}. Figure 3(c) shows the calculated and measured dependence of the degree of linear polarization of the polariton laser emission on the pump current for Device 2. We observe that the calculated linear polarization shows a good agreement with the measured data, in general. One can see that the difference in current density dependence of the linear polarization between devices 1 and 2 is chiefly due to the different spin relaxation and polariton radiative decay rates. The spin relaxation rate and the polariton radiative decay rate is ~ 30% faster and ~ 30% slower respectively, in device 2 as compared to device 1.

We ascribe these differences to the different magnitudes of photonic disorder in the two devices. The value of the peak polarization is ~ 22 % for both devices and is governed by the ratio of the polarization relaxation rate γ and the polariton radiative decay rate Γ_c.The lower is this ratio, the shorter is the time the polariton condensate possesses for relaxation to the lowest energy polarization state. We observe that this ratio and thus the degree of peak polarization is lower than that reported by Levrat *et al.* [34]. The rate of the decrease of the linear polarization beyond the peak depends on the ratio of the nonlinear coefficient α_1 and the linear polarization splitting Ω.

The spatial coherence of the polariton laser emission was measured with a misaligned Mach-Zehnder interferometer (see Supplemental Material [40]). The visibility of the fringes was measured as a function of displacement between two identical images of polariton emission for injection levels below and above the lasing threshold. The measured visibility is plotted as a function of the injection current in Fig. 4(a). A peak visibility of ~ 38 % is recorded above threshold at an injected current density of J = 1.3 J_{th}. While the peak visibility should ideally approach unity at zero displacement between two identical images of the polariton condensate, such high values have not been experimentally reported. This is probably due to quantum fluctuations in the condensate and the fact that the condensate fraction of the polariton gas should be less than 50%, which has been theoretically predicted [44]. The visibility of the fringes is plotted in Fig. 4(b) as a function of displacement between two identical images of the LP emission for injection levels below and above the polariton lasing threshold. The full-width at half maximum (FWHM) of the distribution above threshold is ~ 4 μm, which is the approximate size of the relevant condensate.

In conclusion, we report on detailed steady state measurements of the linear polarization degree of electroluminescence in several diode polariton lasers. The linear polarization build-up is caused by the pinning effect that arises due to the energy splitting of polariton modes polarized along different crystal axes. In addition to the injection dependent linear polarization, we have also studied the polarization resolved output light-current characteristics. A maximum degree of linear polarization of ~ 22 % is observed. The experimental results have been theoretically analyzed by modeling the kinetics of the system with a system of coupled stochastic differential equations. The agreement of theory and experiment is very good, in general. In one of the devices, a surprising and significant lowering of the laser threshold is observed for the polarization resolved output, compared to that for the unresolved output. This effect is believed to be induced by the spatial inhomogeneity in the microcavity due to defects or photonic disorder.

Acknowledgement

This work is supported by the National Science Foundation under the MRSEC program (Grant DMR-1120923). Plasma-assisted molecular beam epitaxial growth of the devices and device fabrication were carried in the Robert H. Lurie Nanofabrication Facility. I. I. acknowledges support of grant MK-5220.2015.2 and from Singaporean Ministry of Education under AcRF Tier 2 grant MOE2015-T2-1-055. A. K. acknowledges support from the EPSRC Programme grant "Hybrid Polaritonics".

References:

1. Q. Ren, R. P. Gailitis, K. P. Thomson, and J. T. Lin, IEEE J. Quant. Electron. **26** , 2284 (1990) ; M. Schadt, K. Schmitt, V. Kozinkov, and V. Chigrinov, Jpn. J. Appl. Phys. **31**, 2155 (1992) ; M. Hasegawa, and Y. Taira, Journal of Photopolymer Science and Technology **8** , 241 (1995) ; N. Kawatsuki, H. Ono, H. Takatsuka, T. Yamamoto, and O. Sangen, Macromolecules **30**, 6680 (1997) ; B. W. Chwirot *et al.*, Lasers Surg. Med. **21**, 149 (1997).
2. A. Imamoglu, R. J. Ram, S. Pau, and Y. Yamamoto, Phys. Rev. A **53**, 4250 (1996).
3. H. Deng, G. Weihs, D. Snoke, J. Bloch, and Y. Yamamoto, Proc. Natl. Acad. Sci. **100**, 15318 (2003).
4. C. Weisbuch, M. Nishioka, A. Ishikawa, and Y. Arakawa, Phys. Rev. Lett. **69**, 3314 (1992).
5. G. Khitrova, H. M. Gibbs, F. Jahnke, M. Kira, and S.W. Koch, Rev. Mod. Phys. **71**, 1591 (1999).
6. D. Porras, C. Ciuti, J. J. Baumberg, and C. Tejedor, Phys. Rev. B **66**, 085304 (2002).
7. Le Si Dang, D. Heger, R. André, F. Bœuf, and R. Romestain, Phys. Rev. Lett. **81**, 3920 (1998).
8. R. Huang, Y. Yamamoto, R. André, J. Bleuse, M. Muller, and H. Ulmer-Tuffigo, Phys. Rev. B **65**, 165314 (2002).

9. M. Richard, J. Kasprzak, R. Romestain, R. André, and L. S. Dang, Phys. Rev. Lett. **94**, 187401 (2005).
10. H. Deng, D. Press, S. Götzinger, G. S. Solomon, R. Hey, K. H. Ploog, and Y. Yamamoto, Phys. Rev. Lett. **97**, 146402 (2006).
11. J. Kasprzak, M. Richard, S. Kundermann, A. Baas, P. Jeambrun, J. M. J. Keeling, F. M. Marchetti, M. H. Szyman´ska, R. Andre´, J. L. Staehli, V. Savona, P. B. Littlewood, B. Deveaud and L. S. Dang, Nature **443**, 409 (2006).
12. R. Balili, V. Hartwell, D. Snoke, L. Pfeiffer, and K. West, Science **316**, 1007 (2007).
13. S. Christopoulos, G. Baldassarri Höger von Högersthal, A. J. D. Grundy, P. G. Lagoudakis, A. V. Kavokin, J. J. Baumberg, G. Christmann, R. Butté, E. Feltin, J.-F. Carlin, and N. Grandjean, Phys. Rev. Lett.**98**, 126405 (2007).
14. G. Christmann, R. Butté, E. Feltin, J. Carlin and N. Grandjean, Appl. Phys. Lett. **93**, 051102 (2008).
15. D. Bajoni, P. Senellart, E. Wertz, I. Sagnes, A. Miard, A. Lemaître, and J. Bloch, Phys. Rev. Lett. **100**, 047401 (2008).
16. S. Kéna-Cohen and S. R Forrest, Nat. Photon.**4**, 371(2010).
17. T. Guillet, M. Mexis, J. Levrat, G. Rossbach, C. Brimont, T. Bretagnon, B. Gil, R. Butté, N. Grandjean, L. Orosz, F. Réveret, J. Leymarie, J. Zúñiga-Pérez, M. Leroux, F. Semond, and S. Bouchoule, Appl. Phys. Lett. **99**, 161104 (2011).
18. F. Li, L. Orosz, O. Kamoun, S. Bouchoule, C. Brimont, P. Disseix, T. Guillet, X. Lafosse, M. Leroux, J. Leymarie, G. Malpuech, M. Mexis, M. Mihailovic, G. Patriarche, F. Réveret, D. Solnyshkov, and J. Zuniga-Perez, Appl. Phys. Lett.**102**, 191118 (2013).

19. S. Azzini, D. Gerace, M. Galli, I. Sagnes, R. Braive, A. Lemaître, J. Bloch, and D. Bajoni, Appl. Phys. Lett. **99**, 111106 (2011).

20. A. Das, J. Heo, M. Jankowski, W. Guo, L. Zhang, H. Deng, and P. Bhattacharya, Phys. Rev. Lett. **107**, 066405 (2011).

21. P. Bhattacharya, B. Xiao, A. Das, S. Bhowmick, and J. Heo, Phys. Rev. Lett. **110**, 206403 (2013).

22. C. Schneider, A. Rahimi-Iman, N. Y. Kim, J. Fischer, I. G. Savenko, M. Amthor, M. Lermer, A. Wolf, L. Worschech, V. D. Kulakovskii, I. A. Shelykh, M. Kamp, S. Reitzenstein, A. Forchel, Y. Yamamoto and S. Hofling, Nature (London) **497**, 348 (2013).

23. J. Heo, S. Jahangir, B. Xiao, and P. Bhattacharya, NanoLett. **13** (6), 2376 (2013).

24. P. Bhattacharya, T. Frost, S. Deshpande, M. Z. Baten, A. Hazari, and A. Das, Phys. Rev. Lett. **112**, 236802 (2014).

25. J. J. Baumberg, A. V. Kavokin, S. Christopoulos, A. J. D. Grundy, R. Butté, G. Christmann, D. D. Solnyshkov, G. Malpuech, G. Baldassarri Höger von Högersthal, E. Feltin, J.-F. Carlin, and N. Grandjean, Phys. Rev. Lett. **101**, 136409 (2008).

26. A. Das, P. Bhattacharya, J. Heo, A. Banerjee, and W. Guo, Proc. Natl. Acad. Sci. **110**, 2735 (2013).

27. M. D. Martín, D. Ballarini, A. Amo, Ł. Kłopotowsi, L. Viña, A. V. Kavokin, and R. André, Phys. Status Solidi C **2**, 3880 (2005).

28. F. P. Laussy, I. A. Shelykh, G. Malpuech, and A. Kavokin, Phys. Rev. B **73**, 035315 (2006).

29. I. A. Shelykh, Yu. G. Rubo, G. Malpuech, D. Solnyshkov, and A. V. Kavokin, Phys. Rev. Lett. **97**, 066402 (2006).
30. M. Combescot, O. Betbeder-Matibet, and R. Combescot, Phys. Rev. Lett. **99**, 176403 (2007).
31. J. Kasprzak, R. André, Le Si Dang, I. A. Shelykh, A. V. Kavokin, Yuri G. Rubo, K. V. Kavokin, and G. Malpuech, Phys. Rev. B **75**, 045326 (2007).
32. E. del Valle, D. Sanvitto, A. Amo, F. P. Laussy, R. André, C. Tejedor, and L. Viña, Phys. Rev. Lett. **103**, 096404 (2009).
33. D. Read, T. C. H. Liew, Y. G. Rubo, and A. V. Kavokin, Phys. Rev. B **80**, 195309 (2009).
34. J. Levrat, R. Butté, T. Christian, M. Glauser, E. Feltin, J.-F. Carlin, N. Grandjean, D. Read, A. V. Kavokin, and Y. G. Rubo, Phys. Rev. Lett. **104**, 166402 (2010).
35. V. G. Sala, F. Marsault, M. Wouters, E. Galopin, I. Sagnes, A. Lemaître, J. Bloch, and A. Amo, Phys. Rev. B **93**, 115313 (2016).
36. M. Z. Baten, T. Frost, I. Iorsh, S. Deshpande, A. Kavokin and P. Bhattacharya, Scientific Reports **104**, 231119 (2015).
37. M. Z. Baten, A. Bhattacharya, T. Frost, I. Iorsh, A. Kavokin and P. Bhattacharya, Appl. Phys. Lett. **108**, 041102 (2016).
38. Ł. Kłopotowski, M.D. Martin, A. Amo, L. Viña, I.A. Shelykh, M.M. Glazov, G. Malpuech, A.V. Kavokin, R. Andre, Solid State Commun. **139**, 511 (2006).
39. K. G. Lagoudakis, T. Ostatnický, A. V. Kavokin, Y. G. Rubo, R. André and B. Deveaud-Plédran, Science **326**, 974 (2009).

40. See Supplementary Material for description of the device fabrication, the sub-threshold strong-coupling characteristics and descriptions of the various measurements.
41. D. Ballarini, A. Amo, L. Viña, D. Sanvitto, M. S. Skolnick, and J. S. Roberts, Appl. Phys. Lett. **90**, 201905 (2007).
42. D. Ballarini, A. Amo, D. Sanvitto, L. Viña, M. S. Skolnick, and J. S. Roberts, Physica E **40**, 2049 (2008).
43. I. Iorsh, M. Glauser, G. Rossbach, J. Levrat, M. Cobet, R. Butté, N. Grandjean, M. A. Kaliteevski, R. A. Abram, and A. V. Kavokin, Phys. Rev. B **86**, 125308 (2012).
44. D. Sarchi and V. Savona, Phys. Rev. B **75**, 115326 (2007).

Figure Captions

Figure 1 (color online) (a) Schematic representation of the double heterostructure GaN microcavity diode (not drawn to scale), (b) schematic representation of edge emission geometry of the polariton laser diode, (c) measured microphotoluminescence spectrum of the GaN microcavity.

Figure 2 (color online) (a) Normal incidence ($k_{||} \sim 0$) LP electroluminescence intensities recorded as a function of injected current density. The solid line represents theoretically calculated values, (b) LP emission linewidth as a function of injected current density, (c) blueshift of the LP electroluminescence peak emission as a function of injected current density, (d) two threshold lasing behavior with the nonlinearities due to polariton and photon lasing, (e) LP ground state occupancy for different $k_{||}$ states as a function of injection, determined from angle-resolved electroluminescence measurements. The dashed lines in (b), (c) and (d) are guides to the eye.

Figure 3 (color online) (a) Polar plots of the normal incidence ($k_{||} \sim 0$) LP electroluminescence intensities recorded as a function of angle of linear analyzer below and above threshold of Device 1 (The single error bar shown in this figure is common to all the corresponding data points), (b) and (c) measured steady-state degree of linear polarization of Device 1 and Device 2, respectively, as a function of injected current density. The solid line represents the theoretically calculated values, (d) polarization-resolved (along 90^o angle of the linear analyzer) and unresolved light-current characteristics of Device 1. The inset shows an enlargement highlighting the different thresholds, (e) polarization-resolved (along 90^o angle of the linear analyzer) and unresolved light-current characteristics of Device 2.

Figure 4 (color online) (a) Interference visibility measured as a function of the injected current density for zero displacement between the double images of the LP emission, the dashed line is a guide to the eye. (b) Interference visibility measured as a function of the displacement between a double image of the polariton condensate below and above the polariton lasing threshold.

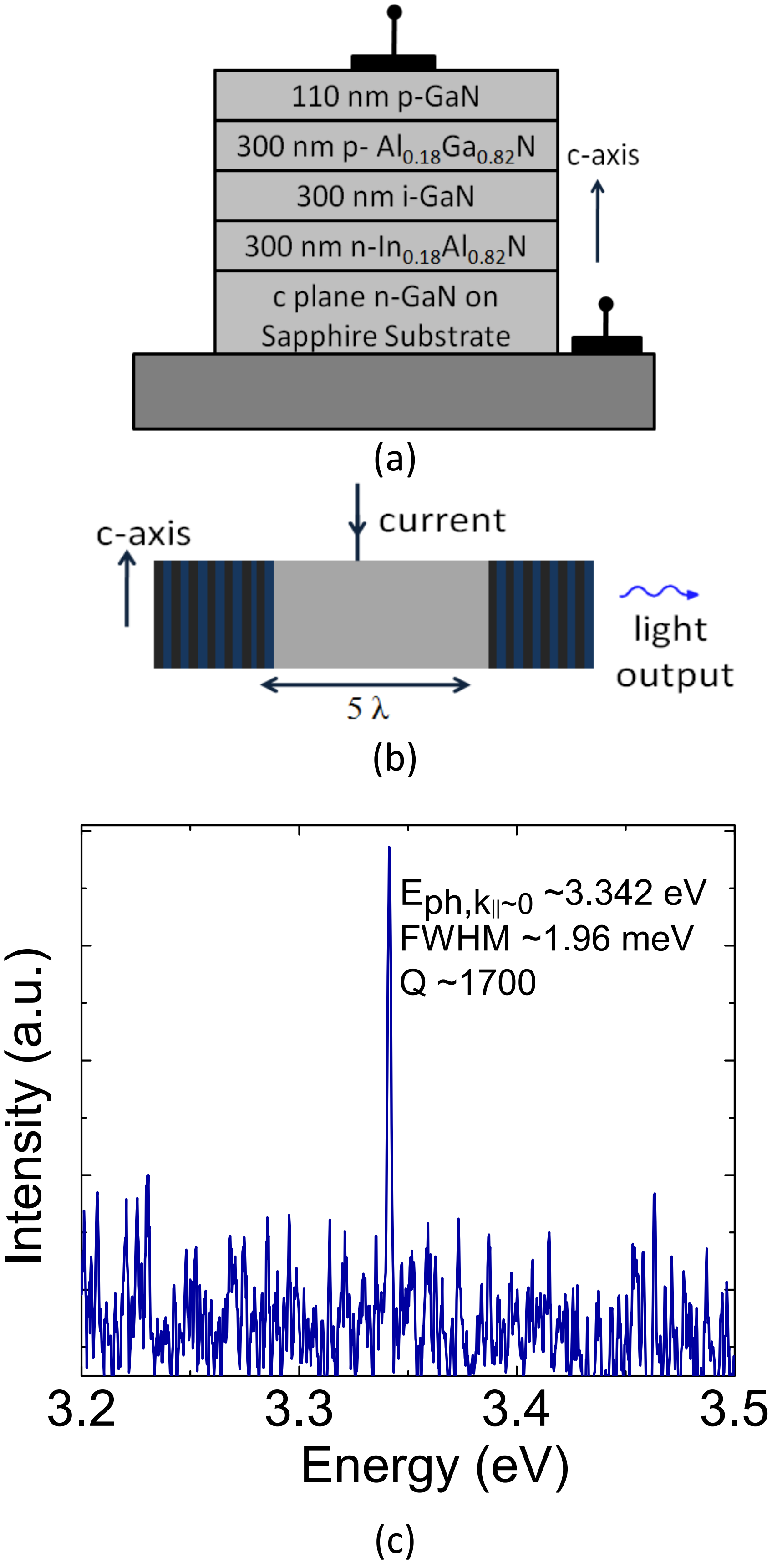

Bhattacharya et al.

Fig. 1

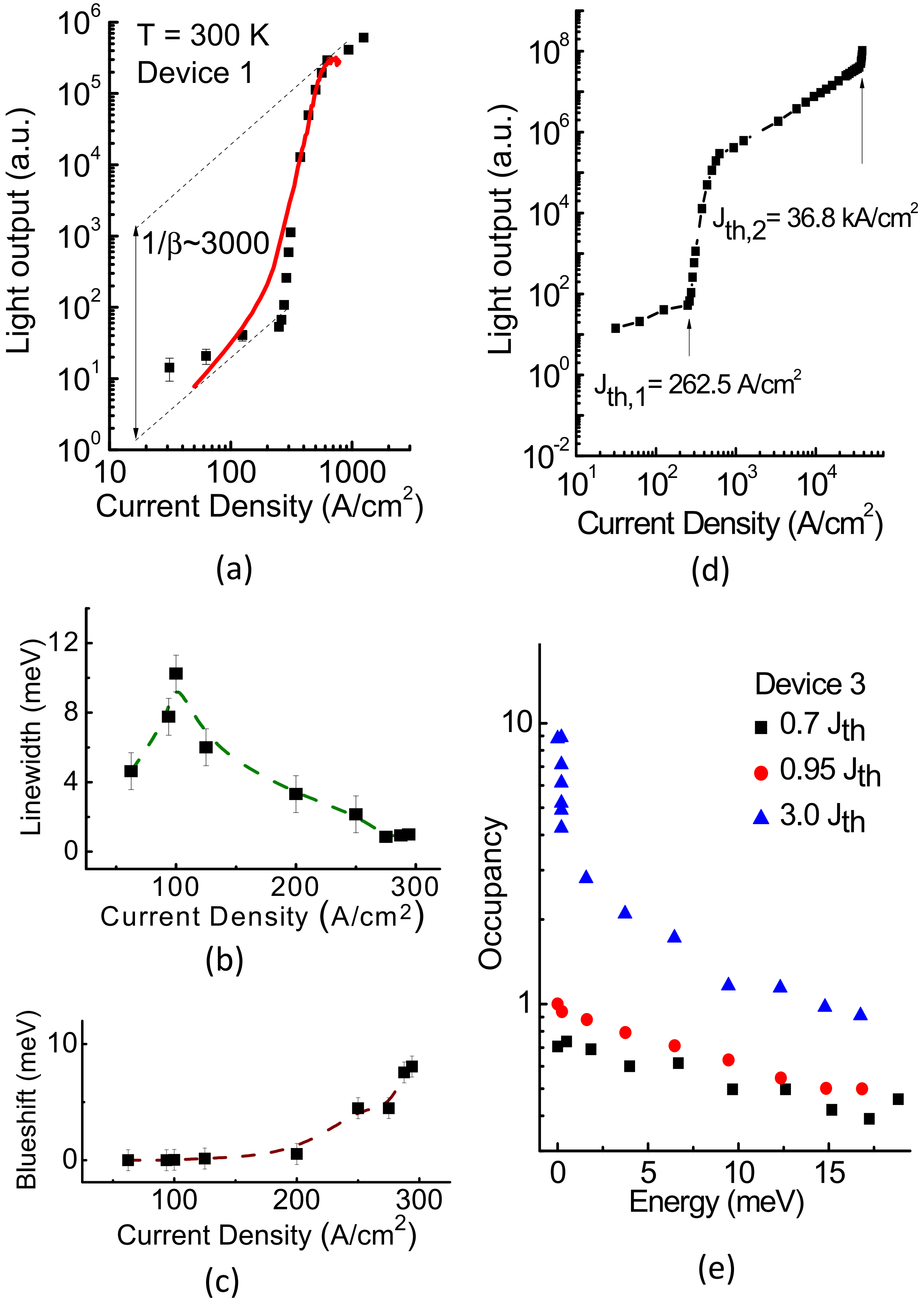

(a)

(d)

(b)

(c)

(e)

Bhattacharya et al.
Fig. 2

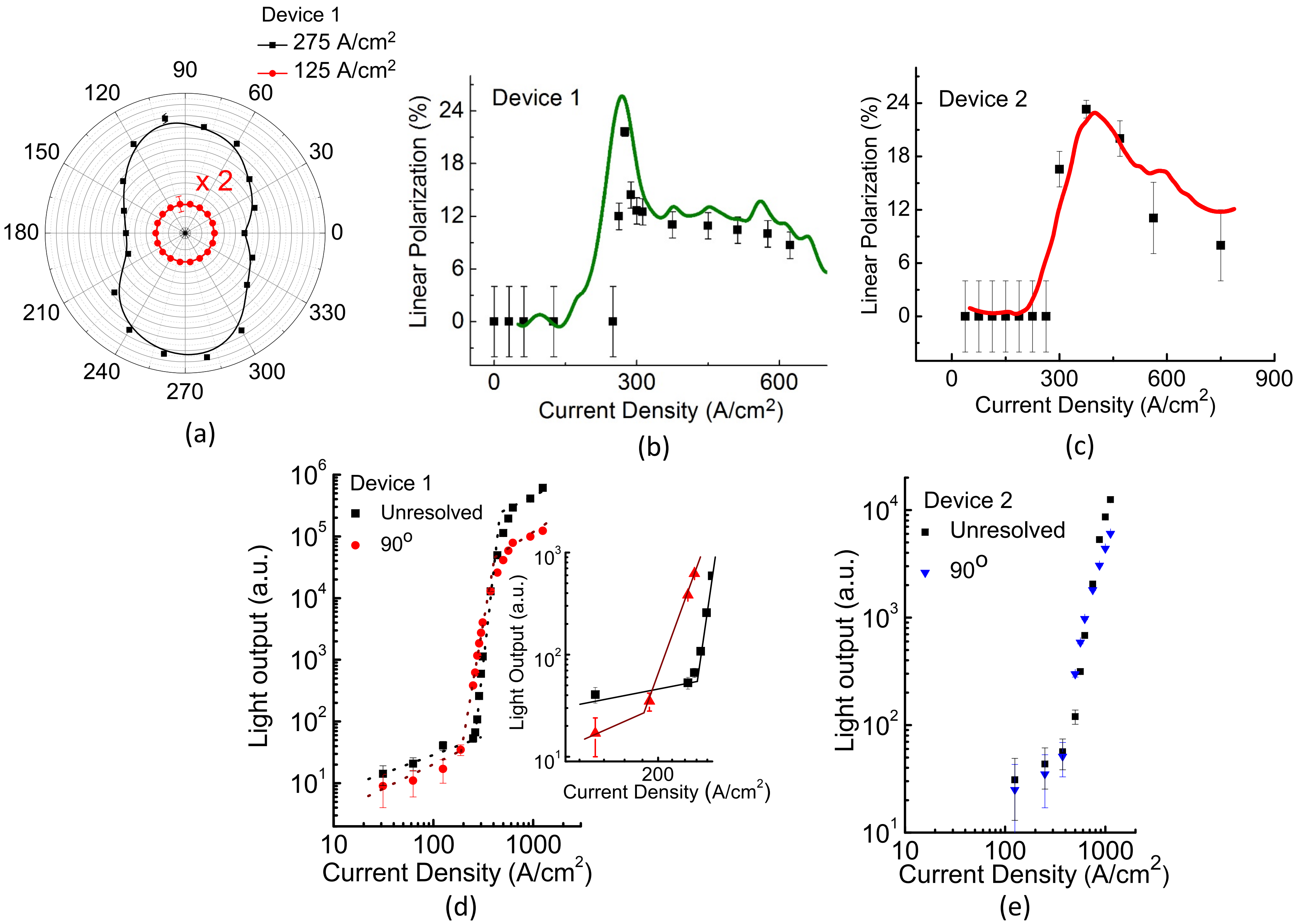

Bhattacharya et al.
Fig. 3

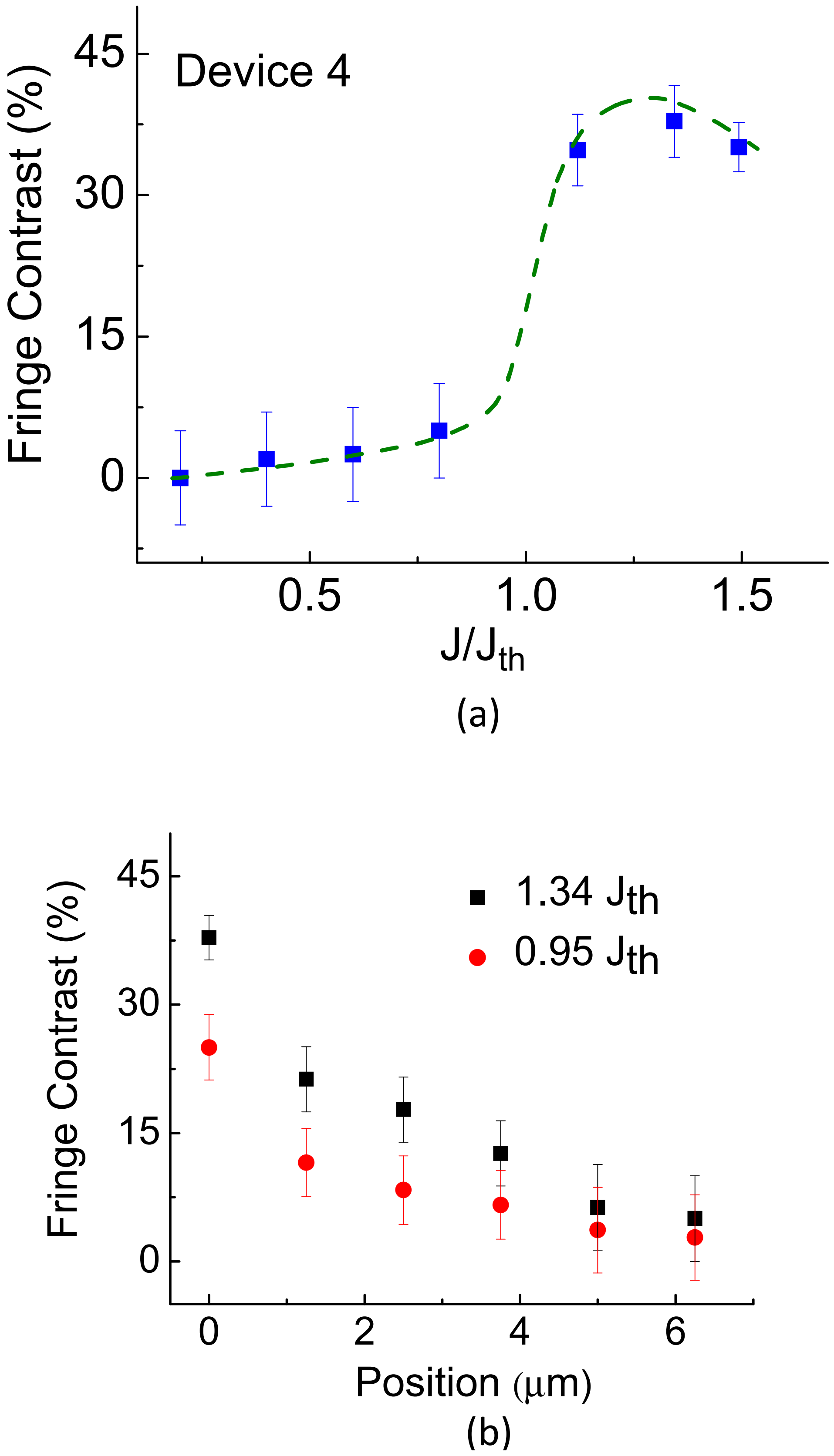

Bhattacharya et al.
Fig. 4